

**MOF-derived nanostructured catalysts for low-temperature ammonia synthesis**

Journal:	<i>Catalysis Science & Technology</i>
Manuscript ID	CY-ART-07-2019-001303.R3
Article Type:	Paper
Date Submitted by the Author:	01-Nov-2019
Complete List of Authors:	Luz Minguez, Ignacio; RTI International, Parvathikar, Sameer; RTI International Carpenter, Michael; RTI International Bellamy, Timothy; RTI International Amato, Kelly; RTI International, Energy Technology Division Carpenter, John; RTI International, Energy Technology Division Lail, Marty; RTI International, Energy Technology Division

ARTICLE

MOF-derived nanostructured catalysts for low-temperature ammonia synthesis

Received 00th January 20xx,
Accepted 00th January 20xx

DOI: 10.1039/x0xx00000x

Ignacio Luz*, Sameer Parvathikar, Michael Carpenter, Timothy Bellamy, Kelly Amato, John Carpenter and Marty Lail*

Nanostructured catalysts for low-temperature ammonia synthesis have been developed via thermal treatment under nitrogen of Ru-containing MOFs. Resulting catalysts reveal high concentration of small Ru nanocrystals (< 4nm) well-dispersed on a graphitic carbon shell demonstrating stable ammonia rates at low temperature. Additional acetylene pre-treatment leads to more dispersed active catalysts containing stable sub-nanometric Ru clusters.

Introduction

Ammonia is vital as an active nitrogen source for important chemicals including fertilizers, polymers, dyes and explosives, and has also been proposed as a futuristic hydrogen storage material.¹ Despite the technological developments within the past century, ammonia production by the conventional Haber-Bosch process over promoted magnetite (Fe₃O₄) catalyst is a high energy and capital-intensive industry due to the high operating temperatures (400-500 °C) and pressures (150-300 bar) required, which results in high energy consumption.² As an alternative process, high ammonia yields of approximately 40-50% have been achieved at lower pressure and temperature conditions (370-400 °C and 50-100 atm) by using Ru-based catalyst supported on graphitic carbon and promoted by combination of alkaline or alkaline-earth metal oxides (such as Na, Cs and Ba), which lower the energy barrier for N₂ dissociation by electron injection (Kellogg advanced ammonia process).^{3,4} Approaches for reducing while stabilizing the Ru crystalline domains as well as for providing better control over the interactions between Ru active surface and promoters are still challenging, which are key factors for the further development of active and stable commercial catalysts for low-temperature ammonia synthesis.

In heterogeneous catalysts, dispersing the catalytically active metallic phase by reducing its crystalline domain down to a few nanometers, or even further to sub-nanometric clusters,⁵ typically leads to an enhancement of the catalytic performance.⁶ Nevertheless, in the absence of strong metal-support interactions to immobilize them, these nanometric

metallic species tend to sinter under reactive environments, thus reducing their active surface area and decreasing catalytic performance over time. Several attempts to provide them with more stability via strong bonding between support and metal,⁷ or even by encapsulation within supports cavities,⁸ have not been sufficient under harsh reaction conditions. Fortunately, a couple of recent approaches revealed excellent stabilization of those metal species, such as trapping them during the crystallization of small pore CHA zeolite (8 member ring window), or covering them with a carbon shell by thermal decomposition of metalorganic precursors,⁹ including metal organic frameworks (MOFs).¹⁰

MOFs have been recently used as versatile precursors for the preparation of advanced heterogeneous catalysts and electrocatalysts.^{11, 12} The versatility of MOFs as precursors is mainly due to their unique and highly tunable features, such as well-defined metal sites spaced by organic struts displayed along a crystalline structure with permanent porosity, which can play two simultaneous roles acting as template and precursor upon applying the proper conditions at high temperature, such as controlled pyrolysis under nitrogen, calcination under air, or reduction under hydrogen.¹³ Upon this transformation, MOFs can lead to well-defined and nanostructured catalytically active species, which are well-dispersed within a microporous carbonaceous matrix.^{14, 15, 16}

In this work, active and stable nanostructured catalysts for low-temperature ammonia synthesis have been developed via thermal treatment under nitrogen of Ru-containing MOFs. The resulting catalysts reveal small Ru nanocrystals (< 4nm) well-dispersed on a graphitic carbon shell demonstrating stable ammonia rates. Furthermore, the addition of a pre-treatment with acetylene leads to more active catalysts containing stable sub-nanometric Ru clusters.

RTI International, 3040 E. Cornwallis Rd, Research Triangle Park, NC 27709, United States

E-mail: iluzminquez@rti.org; mlail@rti.org

† Footnotes relating to the title and/or authors should appear here.

Electronic Supplementary Information (ESI) available: [details of any supplementary information available should be included here]. See DOI: 10.1039/x0xx00000x

Experimental

MOF synthesis

(Ru)HKUST-1 containing 100 % of benzene tricarboxylic acid (RuMOF), and 50 % of benzene tricarboxylic acid and 50 % of pyridine-3,5-dicarboxylic acid (Ru(N)MOF) were prepared according to literature.¹⁷ In a typical synthesis, 1 g of Ru precursor, 600 mg of the appropriate mixture of organic ligands 1,3,5-benzenetricarboxylic acid and pyridine-3,5-dicarboxylic acid, 5 mL of acetic acid and 25 mL of H₂O were loaded into a 100-mL autoclave and heated at 160 °C for 24 hours. The resulting powder was thoroughly washed with H₂O in a filtration funnel and purified in a Soxhlet apparatus with MeOH. All the samples were evacuated at 150 °C under vacuum.

Ru precursor [Ru₂(CH₃COO)₄Cl] was prepared according to literature¹⁸ by mixing 10 gr of RuCl₃·xH₂O (40 wt.% Ru) and 12 g of LiCl (anhydrous), previously evacuated at 80 °C overnight in a vacuum oven, with 70 mL of acetic anhydride and 350 mL of glacial acetic acid. The mixture was stirred and refluxed for 2–4 days until the solution turned into reddish color. After cooling down, the Ru precursor was collected by filtration and was thoroughly washed with acetone.

Characterization

N₂ sorption isotherms. The samples were analysed in a Micromeritics ASAP (Accelerated Surface Area and Porosimetry) 2020 System. Samples were weighted into tubes with seal frits and degassed under vacuum (<500 μm Hg) with heating. Samples were initially heated at 150 °C and held for 4 h, and finally cooled to room temperature and backfilled with N₂. The samples were re-weighted before analysis. The analysis adsorptive was N₂ at 77 K. A multi-point BET surface area was determined from 6 measurements at relative pressures (P/P₀) ranging from 0.05 to 0.30. Single point adsorption total pore volume was measured near saturation pressure (P₀ ≈ 770 mmHg). Adsorption average pore width was also calculated. Pore size distribution plot was determined by Horvath-Kawazoe method using the Cylinder Pore Geometry (Saito-Foley) with Cheng-Yang Correction.

X-ray diffraction. XRD was used to study the crystalline structure of the MOF catalyst. XRD patterns were recorded using a Panalytical Empyrean X-ray diffractometer with Cu Kα radiation (λ=1.54778 Å). The samples were prepared by filling the holder with the dry powder. Crystalline phase stability was investigated using an XRK900 high temperature oven chamber. Sample was first heated in the chamber from 25 °C to 800 °C with a heating rate of 3 °C/min. Diffraction patterns were measured throughout the whole heat treatment using Cu Kα X-ray radiation with a wavelength of 1.5418 Å and a 2θ range of 4.5°–60°. Each pattern was measured for 4 min using a step size and count time of 2θ = 0.0263° and 147 s/step, respectively.

Thermogravimetric analyses (TGA) combined with mass spectrometry (MS) analysis. TGA-MS analyses of the MOF catalysts were performed using a TA Q500 unit coupled to a benchtop quadrupole mass spectrometer (TA).

Raman spectroscopy. Raman analyses were performed on a Horiba XploRA PLUS Confocal Raman Microscope.

CO Chemisorption. CO chemisorption analyses were performed using an AutoChem II 2920 reactor (Micromeritics) equipped with a built-in TCD detector. Samples were activated at 350 °C under 10% H₂/He and were measured under CO at 35 °C.

Transmission electron microscopy (TEM). TEM experiments were performed in a JEOL JEM-2000FX S/TEM microscope with LaB₆ emitter at 200kV with a 120 μm condenser lens aperture and 80 μm objective lens aperture inserted. STEM-HAADF images were acquired in a FEI Titan 80-300 probe aberration corrected scanning transmission electron microscope (STEM) with monochromator.

XPS measurements. X-ray Photoelectron Spectroscopy (XPS) was performed using a monochromatized Al Kα source (hν = 1486.6 eV), operated at 225 W, on a Kratos Axis Ultra DLD with a pass energy for narrow scan spectra of 20 eV, corresponding to an instrument resolution of approximately 600 meV. Survey spectra were collected with a pass energy of 80 eV. Spectral fitting was performed using Casa XPS analysis software. Spectral positions were corrected by shifting the primary C 1s core level position to 285.0 eV, and curves were fitted with quasi-Voigt lines following Shirley background subtraction. The main text of the article should appear here with headings as appropriate.

Catalyst testing

The catalytic performance for ammonia synthesis was tested in a Micromeritics PID Effi Microreactor. The Microreactor is a stand-alone, fully automated system with inlet gas flows metered through mass flow controllers. Feed gases consisted of nitrogen and hydrogen, with argon used as an internal standard. The reactor consisted of a 9mm stainless-steel tube in a furnace. The reactor and the furnace are contained in a hot box, with pressure controlled downstream by a back-pressure regulator. Pressure, temperature and gas flow rates were all controlled by the Microreactor's process control software. The catalyst was diluted with silicon carbide (SiC) in a 1:2 ratio and was placed between two beds of SiC in the reactor, such that the reactor thermocouple was in the middle of the catalyst bed. All catalysts were reduced in 75% H₂/25% N₂ at 370 °C overnight, prior to catalytic activity tests at 95 bar. Downstream of the reactor system, the composition of the process gases was analysed by gas chromatography (for quantifying nitrogen, hydrogen and argon) and MKS MultiGas FTIR Continuous Gas Analyzer (for quantifying ammonia).

Results and discussion

MOF-derived Ru nanostructured catalysts

A series of nanostructured catalysts were developed for ammonia synthesis via controlled pyrolysis of microporous (Ru)HKUST-1 under nitrogen at increasing temperatures up to 900 °C. The resulting catalysts exhibit high concentration of Ru nanocrystals (up to 80 wt.%) homogeneously dispersed and

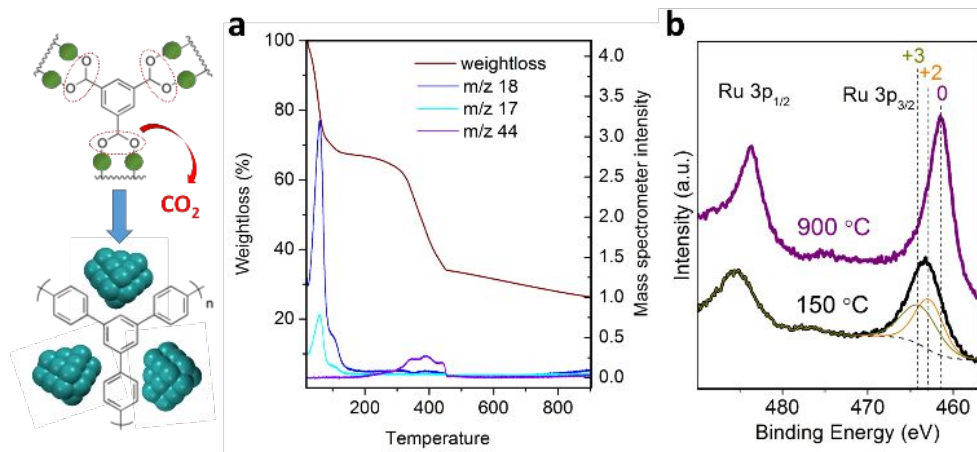


Fig. 1 a) TGA-MS analysis of the transformation treatment of MOF precursor into nanostructured catalysts. b) XPS analysis of the Ru_{3p} signal for MOF precursor (150 °C) and nanostructured catalysts (900 °C).

stabilized along a porous carbon scaffold. The transformational mechanism occurring during pyrolysis of the MOF precursor was elucidated via combination of characterization techniques,

such as Cu, Co or Fe, under the presence of carbonaceous species acting as reducing agent.¹⁶

As shown in Fig. 2a, *in situ* XRD monitoring of the MOF

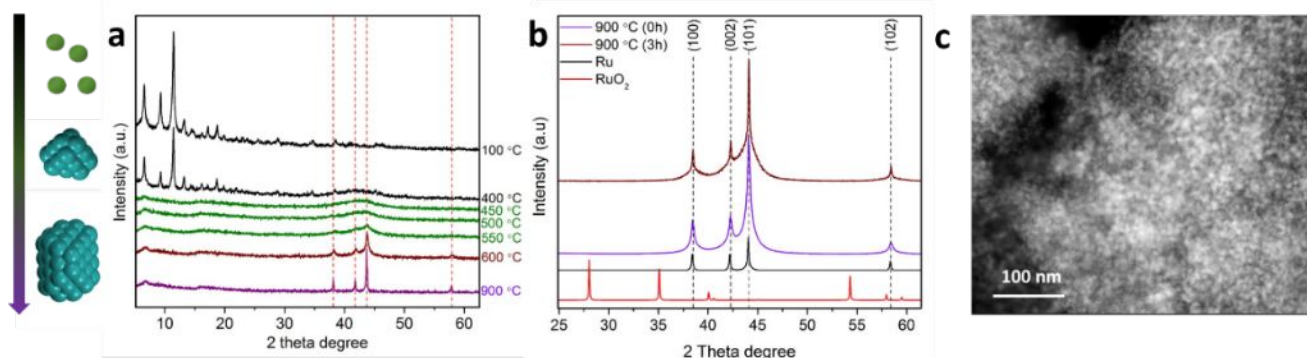


Fig. 2 a) *In situ* XRD monitoring of the transformation of MOF precursor into nanostructured catalysts. b) XRD pattern of catalysts obtained at 900 °C at varying holding time (0 and 3 h) compared to Ru and RuO₂ crystalline patterns. c) STEM-HAADF image of nanostructured catalysts.

such as X-ray diffraction (XRD), X-ray photoelectron spectroscopy (XPS), thermogravimetry coupled to mass spectroscopy (TGA-MS), scanning-transmission electron microscopy (STEM), Raman spectroscopy, N₂ sorption isotherms and CO pulse chemisorption. This understanding enables the optimization of the physicochemical properties of the resulting nanostructured Ru catalysts in terms of nanocrystal size, surface area and level of graphitization, which have a crucial impact on their reaction rates and long-term stability.

Monitoring the thermal transformation of MOF precursor by TGA-MS (Fig. 1a) shows the release of CO₂ molecules between 200 and 450 °C, consistent with decarboxylation of benzene- and pyridine-tricarboxylic acid linkers. This may lead to the aggregation of Ru dimers into clusters while decarboxylated phenyl rings are converted into an amorphous carbonaceous matrix, as previously proposed for carboxylate-containing MOF-5.¹⁹ XPS analysis of the resulting metal clusters confirms the complete reduction to metallic Ru nanocrystals of the MOF precursor (Fig. 1b). The direct reduction of Ru^{2+/3+} into Ru⁰ under these conditions is characteristic of elements having positive reduction potential,

transformation into Ru nanostructured catalyst as function of temperature reveals an advanced attenuation of the characteristic diffraction peaks corresponding to the MOF crystalline structure between 400-450 °C. An amorphization of the MOF crystalline phase may occur at this temperature range followed by the appearance of broad diffraction peaks between 2θ = 35-50° corresponding to metallic Ru crystalline phase. The broadness of the signals suggests the initial formation of sub-nanometric clusters upon full decarboxylation which evolve into larger Ru nanocrystals with temperature, as the diffraction peaks are converging into sharper peaks, such as the one centered at 2θ = 44° attributed to the Ru crystalline plane (101). At 900 °C, dwelling time promotes the aggregation of the small nanocrystals into larger as indicated by the progressive sharpening of the diffraction peaks (see Fig 2b). This Ru nanocrystal sintering is attributed to a rearrangement of the carbonaceous matrix, as discussed in more detail below (see Fig. 3). The absence of additional XRD peaks (such as RuO₂) also confirms the full reduction of cationic Ru^{2+/3+} into metallic Ru⁰ during the pyrolytic transformation, thus supporting the results obtained by XPS. STEM analysis of the material obtained at 900 °C with no

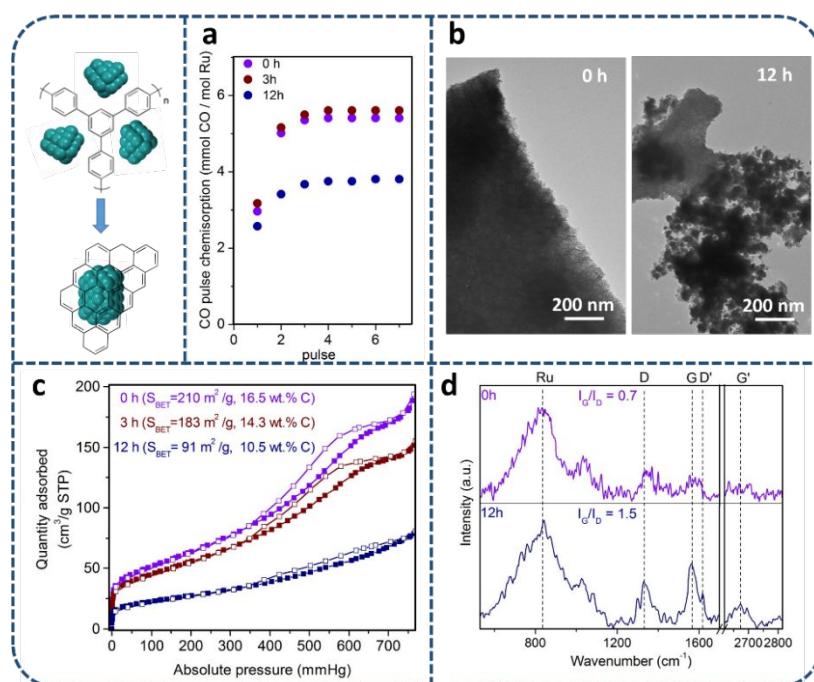


Fig. 3 (a) CO chemisorption at 35 °C, (b) TEM analysis, (c) N₂ sorption isotherms at 77K (BET surface area and carbon elemental analysis), and (d) Raman spectra for MOF-derived catalysts obtained by pyrolysis at 900 °C and different holding times (0, 3 and 12 h).

holding time (0h) reveals high concentration of well-dispersed small Ru nanocrystals (85% of Ru, see Fig. S1), suggesting the existence of a thin carbonaceous matrix separating the nanocrystals. A close look at the nanostructure by STEM suggests the existence of a multilayered graphitic carbon scaffold stabilizing the Ru nanocrystals, as identified by the typical spacing for a multilayered structures (0.4 nm) as well as the presence of graphitic carbon confirmed by Raman spectroscopy (Fig. 3d) and elemental mapping analysis (see Fig. 3d and S1). This specific nanostructure has been recently reported for other MOF-derived materials, such as CoMOF-74.²⁰

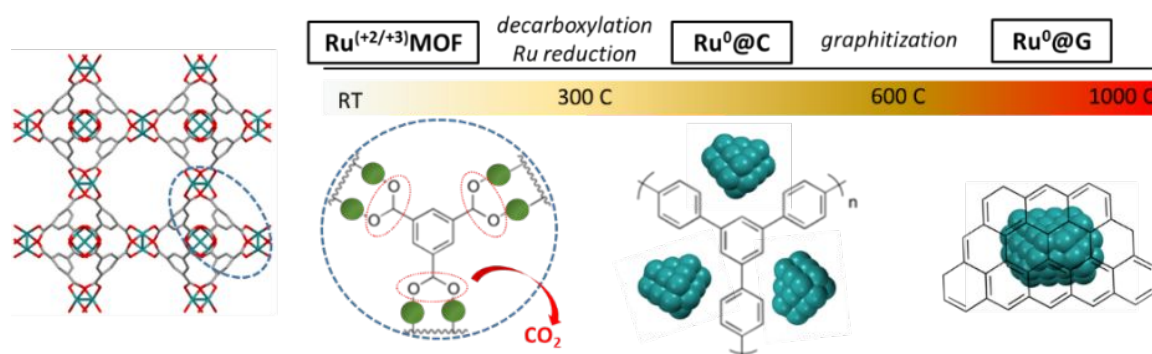
In order to provide more insight about the effect of holding the pyrolysis temperature on the nanostructure of the Ru nanocrystals as well as the nature of the carbonaceous matrix acting as support, samples treated at 900 °C for different holding times (0, 3 and 12h) were characterized by a combination of techniques, such as TEM, N₂ sorption isotherms, CO chemisorption, Raman and elemental analysis. Long holding times during pyrolysis (12h) lead to the partial sintering of Ru nanocrystals accompanied by apparent changes in the composite morphology (see Fig. 3b and Fig. S2). According to the results obtained by CO pulse chemisorption, holding times higher than 3 hours result in reduction of the active surface (Fig. 3a) due to the aforementioned Ru sintering. Catalyst surface area and pore size distribution also decreases from 210 m²/g for 0 h, to 183 or 91 m²/g for 3 or 12 h, respectively (Fig. 3c and Fig. S3). This suggests a rearrangement of the carbon into a less porous (but more stable) morphology which is involving a proportional loss of carbon (each sample contains 16.5, 14.3 and 10.5 wt.% C,

respectively). In the same way, full release of hydrogen also indicates the advanced fusion of benzylic rings into 2D-graphitic structures even at low holding times (0h), as determined by elementary analysis.

As shown in Fig. 3d, Raman spectra of the MOF-derived catalysts exhibit two peaks located at 1326 and 1562 cm⁻¹, which are attributed to vibration bands of carbon in disordered graphite (D band) and the E_{2g} mode of the graphite (G band).²¹ The G to D band intensity ratio (I_G/I_D) is normally used to assess the crystalline structure of the graphitic carbon. This result reveals that the crystallinity and also the concentration (intensity of the peaks) of graphitic carbon in the catalyst improves by holding for longer time (12 h) at 900 °C, as I_G/I_D ratio increases from 0.7 for no holding (0h) to 1.5 for 12 h. This supports the hypothesis that the loss of catalyst surface area as a function of holding time may be explained by a carbon rearrangement into more ordered graphitic carbon. Better definition and higher intensity of the Raman signals G and D at longer holding times is consistent with the removal of non-stable amorphous carbonaceous species, reducing the background signal and the carbon contained therein.

Mechanism of formation of MOF-derived nanostructured catalyst

As illustrated in Scheme 1, the hypothetical mechanism for the thermal transformation of (Ru)HKUST-1 into Ru nanostructured catalysts under inert conditions involves first, the progressive cleavage of the carboxylate group and release of CO₂ between 200–400 °C¹², which may lead to formation of metallic Ru sub-nanometric clusters embedded within a thin amorphous carbonaceous matrix resulting from the polymerization of the benzylic rings. Subsequently, the Ru sub-



Scheme 1. Transformational mechanism of (Ru)HKUST-1 precursor into nanostructured catalysts.

nanometric clusters may start sintering to form larger nanocrystals between 400-600°C, which are still well-dispersed on the microporous amorphous carbon matrix. Finally, the amorphous carbonaceous matrix may be progressively rearranged into multilayer graphitic carbon at 900 °C, which leads to a material exhibiting lower carbon content and lower surface area, but more order, after long holding times (12 h).

Stability of MOF-derived Ru nanostructured catalysts for ammonia synthesis

The thermal and chemical stability of MOF-derived catalysts has been evaluated under ammonia synthesis conditions for 4 hours (H_2 at 400 °C) by in-situ and ex-situ characterization techniques, such as TEM, Raman and XRD. TEM analysis of the material before and after exposure to reaction conditions reveals a morphological change in terms of the apparent Ru nanocrystal size. After H_2 activation, Ru nanocrystals for the sample prepared with 0 h holding time seems to be smaller (3-4 nm) than as-synthesized materials (6-7 nm). Furthermore, Raman spectroscopy shows better definition and higher intensity of the signals after the H_2 activation (Fig. 4b) while thermo-XRD reveals no change on the size of the crystalline domain (Fig. 4c). The combination of these results suggest that only amorphous carbonaceous species are released during the H_2 activation, as Raman relative intensities and the Ru nanocrystal size are maintained during the treatment. Evidence for amorphous carbon loss is obtained by mass spectroscopy detection of a small amount of CH_4 during the activation stage of CO pulsed-chemisorption

experiments, which lead to the enhancement of the available Ru sites upon H_2 activation (see Fig. S4). This finding supports the hypothesis that the Ru active species catalyse the methanation of the non-stable amorphous carbon under reaction conditions, which lead to a highly stable catalyst composed by 3-4 nm Ru nanocrystals stabilized by highly pure graphitic carbon.

Catalytic performance of MOF-derived Ru nanostructured catalysts for ammonia synthesis

MOF-derived catalysts were promoted with Ba and Cs salts following literature reports for other carbon-supported Ru catalysts.²² Ru:Ba:Cs promotion ratio of 1:0.05:0.2 was found optimal for achieving the highest ammonia production rate at 350 °C, gas hourly space velocity (GHSV) of 15,000 h^{-1} and 95 barg. (Table S1). The reaction was also carried out with the optimal promotion at higher GHSVs (30,000 and 60,000 h^{-1}) to eliminate equilibrium constraints, as shown in Fig. S5 and S7. MOF-derived nanostructured catalysts show ammonia production rates per gram of catalyst *ca* 5 $g_{NH_3} g_{cat}^{-1} h^{-1}$ (see Table S3), similar to some of the best Ru catalyst that have been used for commercial ammonia production, such as Ba-Cs-Ru/C.^{4, 23} This production rates per gram of catalyst are attributed to the high concentration of well-dispersed Ru nanocrystals, which is crucial to reduce the reactor dimensions compared to catalysts exhibiting low Ru loadings.

In order to probe the potential of the graphitic carbon environment to improve the catalytic performance of RuMOF-derived catalysts, we also evaluated two alternative approaches to reduce and preserve the metal nanocrystal size of MOF-derived materials. In the first approach, RuMOF precursor is doped with nitrogen via incorporation of defective ligands, and second, RuMOF precursor is pre-treated with C_2H_4 at 500 °C prior to the pyrolytic treatment at 900 °C with N_2 .

Alternative MOF precursors: N-containing (Ru)HKUST-1

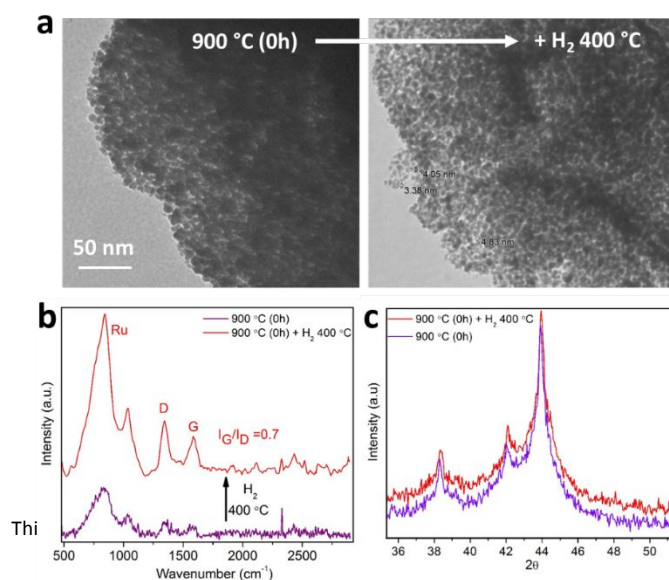


Fig. 4 Ru nanostructured catalyst stability under ammonia synthesis conditions characterized by TEM (a), Raman (b) and thermo-XRD (c).

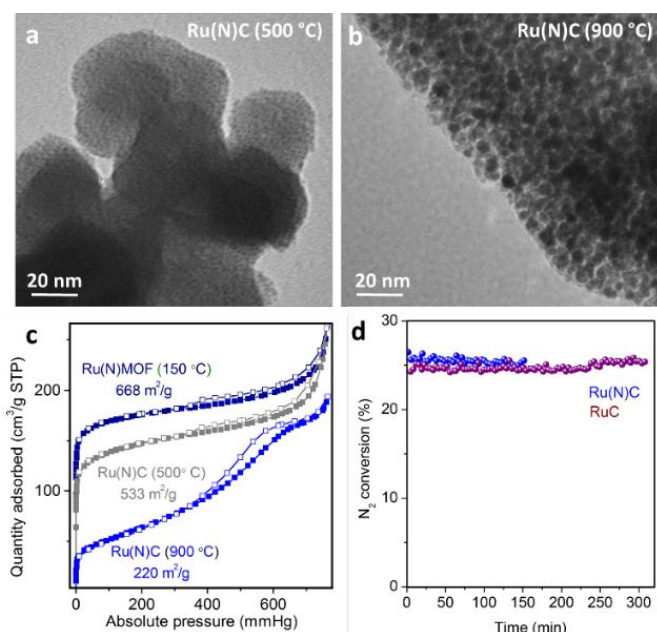


Fig. 5 TEM images of nanostructured catalysts prepared from alternative Ru(N)MOF precursors at a) 500 °C and b) 900 °C. c) Effect of the temperature of the treatment on the N₂ sorption isotherms at 77K. d) N₂ conversion for Ru(N)MOF with RuMOF at 350 °C and 95 barg.

According to literature,¹⁴ the presence of N-containing ligands in MOF precursors provides improved stabilization of sub-nanometric metal clusters upon pyrolysis. Here, the pyrolysis of defect-engineered (Ru)HKUST-1 (Ru(N)MOF) with a combination of ligands (3,5-pyridinedicarboxylate and 1,3,5-pyridinetricarboxylate¹⁷) has been evaluated as an alternative route to obtain smaller Ru nanocrystals, and therefore, more active MOF-derived catalysts. As shown in Fig. 5, TEM analysis reveals the presence of sub-nanometric Ru clusters for the Ru(N)MOF precursor pyrolyzed at 500 °C compared to the N-free MOF precursor exhibiting nanocrystals of 2-3 nm. In addition, the surface area of the material containing N ligands (533 m²/g) is more than 2 times greater than in the case of the N-free MOF pyrolyzed at 500 °C (250 m²/g). Therefore, this confirms the role of N-doped carbonaceous species as excellent stabilizers of sub-nanometric Ru clusters during the early stage of the thermal transformation (between 400-600 °C).

Unfortunately, pyrolysis of Ru(N)MOF precursor at 900 °C, which is required for the carbon graphitization, leads to less porous materials (200 m²/g) exhibiting larger Ru nanocrystals (2-3 nm). This may be caused by the carbon rearrangement during graphitization at 900 °C, as seen for N-free RuMOF precursor. Promotion with barium and cesium leads to catalysts with similar activity levels as the N-free RuMOF catalysts as demonstrated in Fig. 5d. Additionally, the Ru(N)MOF-derived catalysts showed higher deactivation (3%/h) compared to RuMOF catalysts (0.3%/h). Unfortunately, the stability test performed over Ru(N)C material prepared at 500 °C (without additional treatment at 900 °C) under ammonia synthesis conditions lead to full degradation of the

non-graphitic matrix and sintering of the sub-nanometric Ru domains. Nevertheless, this highly dispersed Ru catalyst may be stable for other heterogeneously catalyzed reactions operating at lower temperatures.

Acetylene pretreatment

Acetylene deposition has been well studied for the preparation of carbon nanotubes or carbon-encapsulated metal particles.²⁴ Recently, the use of acetylene deposition on the pores of MOFs resulted in an efficient approach for the precisely-controlled manufacture of ultra-small metal nanoparticles within porous carbon shells (core/shell metal/C).²⁰ As shown in Fig. 6, the pre-treatment of RuMOF precursor with acetylene at 500 °C resulted in the formation of carbonaceous species filling the MOF micropores, which

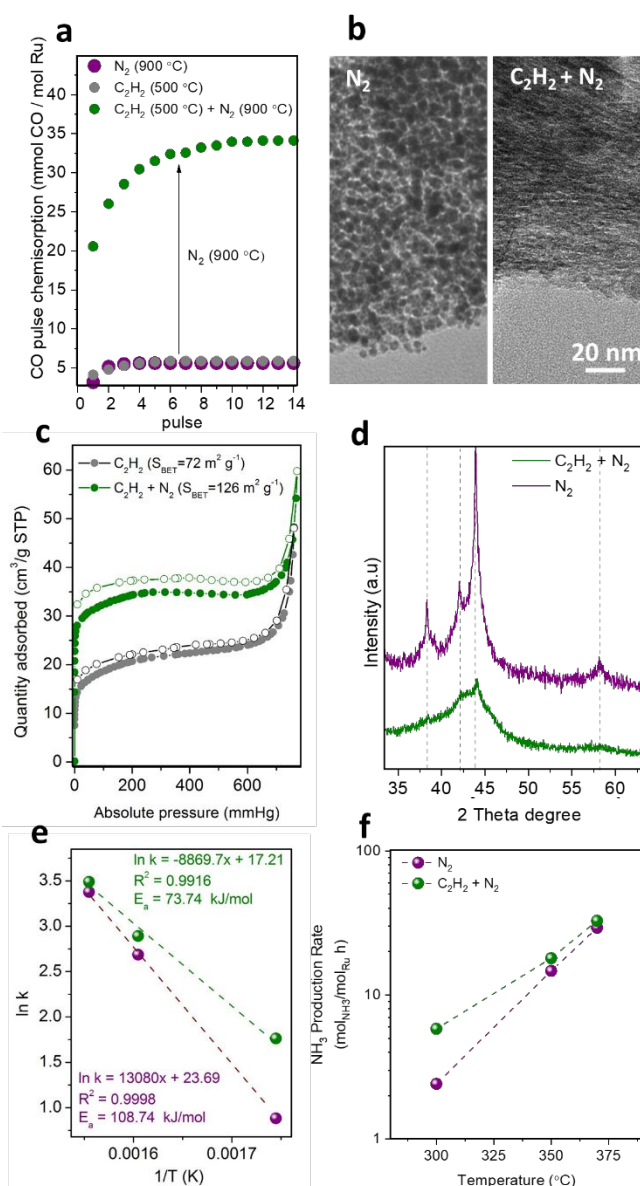


Fig. 6 (a) CO chemisorption at 35 °C, (b) TEM analysis, (c) N₂ sorption isotherms at 77K, (d) XRD pattern, (e) activation energy, and (f) ammonia production rates for MOF-derived catalysts treated with C₂H₂ at 500 °C (grey), treated with C₂H₂ at 500 °C and also N₂ at 900 °C (green), and only treated with N₂ at 900 °C (purple).

stabilize sub-nanometric Ru clusters upon pyrolysis at 900 °C under N₂ in contrast to non-pre-treated samples (Fig. 6b).

CO chemisorption study reveals that the pyrolytic treatment at 900 °C is crucial to uncover the available active surface of Ru (Fig 6a), which also leads to an increment of the surface area (Fig 6c). This can be attributed to the release of amorphous carbon species that were blocking the Ru surface. The stabilization of the sub-nanometric Ru clusters via acetylene pre-treatment was confirmed by TEM and XRD. TEM images in Fig. 6b highlight the effect of the additional acetylene pre-treatment on reducing the Ru particle size, as suggested by the absence of larger Ru nanocrystals (> 1nm). This is supported by the highly broad XRD diffraction peaks collected for acetylene-treated samples (Fig. 6d). As shown in Fig. 6e,f and Table S2, this increment on the active surface area of the C₂H₂-treated catalysts resulted in a 2-fold enhancement on the catalytic activity. For instance, TOF 50·10⁻³ s⁻¹ vs 20·10⁻³ s⁻¹ at 430 °C, and 1.6·10⁻³ s⁻¹ vs 0.7·10⁻³ s⁻¹ at 300 °C were measured for RuC (C₂H₂+N₂) vs RuC (N₂) respectively.

This result shows that the enhancement of ruthenium active surface (Fig 6a) by reducing the particle size does not result in a proportional enhancement of the catalytic activity. This suggests that the accessibility of the gas reagents to the active sites may be reduced by mass transport limitations within the bulky catalyst particle. This limitation can be overcome by further pre-dispersing MOF nanocrystals on a stable support prior carbonization, as recently demonstrated by our group for transformation of single MOF nanocrystals into single nanostructured catalysts^{13, 25}. Moreover, the activity of MOF-derived catalysts may still be limited by the N₂ dissociation step occurring over the promoter surface rather than the hydrogenation step over Ru active sites, as recently demonstrated by the use of barium-doped calcium amides (Ba-Ca(NH₂)₂) as dual support/promoter (Table S3).²⁶

Conclusions

Active and stable nanostructured Ru catalyst for low-temperature ammonia synthesis have been developed via pyrolytic treatment of Ru containing MOFs. The optimization of the thermal treatment conditions resulted in small Ru nanocrystals (<4nm) well-dispersed on a graphitic carbon matrix demonstrating good activity and stability for ammonia synthesis. An additional pretreatment with acetylene allows to stabilize smaller and more active sub-nanometric Ru clusters upon an additional pyrolytic treatment at 900 °C in N₂ required to release the available catalytically active surface. This two-step strategy provides an efficient and general route to develop highly stable and active MOF-derived heterogeneous catalyst, serving as a versatile platform to improve the interactions between Ru active surface and alkaline/alkaline-earth promoters via atomic design of the proper multi-metallic MOF precursors.

Conflicts of interest

There are no conflicts to declare.

Acknowledgements

The authors gratefully acknowledge the support from the U.S Department of Energy's Advanced Research Project Agency Energy (ARPA-E) Renewable Energy to Fuels Through Utilization of Energy-Dense Liquids (REFUEL) program (DE-AR-0000811). The authors would also like to acknowledge to Mr. Ching-Chang Chung, Mr. Rohan Dhall and Mr. Fred Stevie from the Analytical Instrumentation Facility, College of Engineering, North Carolina State University (Raleigh, NC).

References

1. S. Satyapal, J. Petrovic, C. Read, G. Thomas and G. Ordaz, *Catal. Today*, 2007, **120**, 246-256; A. Klerke, C. H. Christensen, J. K. Nørskov and T. Vegge, *J. Mater. Chem.*, 2008, **18**, 2304-2310.
2. N. Saadatjou, A. Jafari and S. Sahebdehfar, *Chem. Eng. Commun.*, 2015, **202**, 420-448.
3. Z. Kowalczyk, S. Jodzis and J. Sentek, *Appl. Catal., A*, 1996, **138**, 83-91; R. Schlogl, *Angew. Chem., Int. Ed.*, 2003, **42**, 2004-2008.
4. H. Bielawa, O. Hinrichsen, A. Birkner and M. Muhler, *Angew. Chem., Int. Ed.*, 2001, **40**, 1061-+.
5. J. Oliver-Meseguer, J. R. Cabrero-Antonino, I. Dominguez, A. Leyva-Perez and A. Corma, *Science*, 2012, **338**, 1452-1455.
6. L. Liu and A. Corma, *Chem. Rev.*, 2018, **118**, 4981-5079.
7. S. T. Hunt, M. Milina, A. C. Alba-Rubio, C. H. Hendon, J. A. Dumesic and Y. Román-Leshkov, *Science*, 2016, **352**, 974-978; H. Tang, J. Wei, F. Liu, B. Qiao, X. Pan, L. Li, J. Liu, J. Wang and T. Zhang, *J. Am. Chem. Soc.*, 2016, **138**, 56-59.
8. C. P. Canlas, J. Lu, N. A. Ray, N. A. Grosso-Giordano, S. Lee, J. W. Elam, R. E. Winans, R. P. Van Duyne, P. C. Stair and J. M. Notestein, *Nature Chem.*, 2012, **4**, 1030; J. Lu, B. Fu, M. C. Kung, G. Xiao, J. W. Elam, H. H. Kung and P. C. Stair, *Science*, 2012, **335**, 1205-1208; G.-H. Wang, J. Hilgert, F. H. Richter, F. Wang, H.-J. Bongard, B. Spliethoff, C. Weidenthaler and F. Schüth, *Nat. Mater.*, 2014, **13**, 293.
9. L. Liu, P. Concepción and A. Corma, *J. Catal.*, 2016, **340**, 1-9; K. J. Lee, Y. J. Sa, H. Y. Jeong, C. W. Bielawski, S. H. Joo and H. R. Moon, *Chem. Commun.*, 2015, **51**, 6773-6776.
10. H.-L. Jiang, B. Liu, Y.-Q. Lan, K. Kuratani, T. Akita, H. Shioyama, F. Zong and Q. Xu, *J. Am. Chem. Soc.*, 2011, **133**, 11854-11857; S. Dang, Q.-L. Zhu and Q. Xu, *Nat. Rev. Mater.*, 2017, **3**, 17075; B. Liu, H. Shioyama, T. Akita and Q. Xu, *J. Am. Chem. Soc.*, 2008, **130**, 5390-5391.
11. J. L. Shui, C. Chen, L. Grabstanowicz, D. Zhao and D. J. Liu, *Proc. Natl. Acad. Sci. U. S. A.*, 2015, **112**, 10629-10634; X. W. Liu, T. J. Sun, J. L. Hu and S. D. Wang, *J. Mater. Chem. A*, 2016, **4**, 3584-3616; K. Shen, X. D. Chen, J. Y. Chen and Y. W. Li, *ACS Catal.*, 2016, **6**, 5887-5903; X. Sun, A. I. O. Suarez, M. Meijerink, T. van Deelen, S. Ould-Chikh, J. Zečević, K. P. de Jong, F. Kapteijn and J. Gascon, *Nat. Commun.*, 2017, **8**, 1680; K. J. Lee, J. H. Lee, S. Jeoung and H. R. Moon, *Acc. Chem. Res.*, 2017; A. Dokania, A. Ramirez, A. Bavykina and J. Gascon, *ACS Energy Lett.*, 2019, **4**, 167-176; T. A. Wezendonk, V. P. Santos, M. A.

- Nasalevich, Q. S. E. Warringa, A. I. Dugulan, A. Chojecki, A. C. J. Koeken, M. Ruitenbeek, G. Meima, H.-U. Islam, G. Sankar, M. Makkee, F. Kapteijn and J. Gascon, *ACS Catal.*, 2016, **6**, 3236-3247.
12. I. Agirrezabal-Telleria, I. Luz, M. A. Ortuño, M. Oregui-Bengoechea, I. Gandarias, N. López, M. A. Lail and M. Soukri, *Nat. Commun.*, 2019, **10**, 2076.
13. I. Luz, M. Soukri and M. Lail, *Chem. Commun.*, 2018, **54**, 8462-8465.
14. S. Ji, Y. Chen, Q. Fu, Y. Chen, J. Dong, W. Chen, Z. Li, Y. Wang, L. Gu, W. He, C. Chen, Q. Peng, Y. Huang, X. Duan, D. Wang, C. Draxl and Y. Li, *J. Am. Chem. Soc.*, 2017; X. Wang, W. Chen, L. Zhang, T. Yao, W. Liu, Y. Lin, H. Ju, J. Dong, L. Zheng, W. Yan, X. Zheng, Z. Li, X. Wang, J. Yang, D. He, Y. Wang, Z. Deng, Y. Wu and Y. Li, *J. Am. Chem. Soc.*, 2017, **139**, 9419-9422.
15. J. Tang, R. R. Salunkhe, H. Zhang, V. Malgras, T. Ahamad, S. M. Alshehri, N. Kobayashi, S. Tominaka, Y. Ide, J. H. Kim and Y. Yamauchi, *Scientific Reports*, 2016, **6**, 30295; R. Lippi, S. C. Howard, H. Barron, C. D. Easton, I. C. Madsen, L. J. Waddington, C. Vogt, M. R. Hill, C. J. Sumbly, C. J. Doonan and D. F. Kennedy, *J. Mater. Chem. A*, 2017, **5**, 12990-12997; W. Cao, W. Luo, H. Ge, Y. Su, A. Wang and T. Zhang, *Green Chem.*, 2017, **19**, 2201-2211.
16. R. Das, P. Pachfule, R. Banerjee and P. Poddar, *Nanoscale*, 2012, **4**, 591-599.
17. O. Kozachuk, I. Luz, F. X. Llabrés i Xamena, H. Noei, M. Kauer, H. B. Albada, E. D. Bloch, B. Marler, Y. Wang, M. Muhler and R. A. Fischer, *Angew. Chem., Int. Ed.*, 2014, **53**, 7058-7062.
18. M. Mukaida, T. Nomura and T. Ishimori, *Bull. Chem. Soc. Jpn.*, 1967, **40**, 2462-+.
19. L. Zhang and Y. H. Hu, *J. Phys. Chem. C*, 2010, **114**, 2566-2572.
20. C. Zhang, X. Guo, Q. Yuan, R. Zhang, Q. Chang, K. Li, B. Xiao, S. Liu, C. Ma, X. Liu, Y. Xu, X. Wen, Y. Yang and Y. Li, *ACS Catal.*, 2018, 7120-7130.
21. L. M. Malard, M. A. Pimenta, G. Dresselhaus and M. S. Dresselhaus, *Phys. Rep.*, 2009, **473**, 51-87.
22. Z. Kowalczyk, M. Krukowski, W. Raróg-Pilecka, D. Szmigiel and J. Zielinski, *Appl. Catal., A*, 2003, **248**, 67-73.
23. C. Liang, Z. Wei, Q. Xin and C. Li, *Appl. Catal., A*, 2001, **208**, 193-201.
24. A. K. M. Fazle Kibria, Y. H. Mo, K. S. Nahm and M. J. Kim, *Carbon*, 2002, **40**, 1241-1247; T.-C. Liu and Y.-Y. Li, *Carbon*, 2006, **44**, 2045-2050.
25. I. Luz, M. Soukri and M. Lail, *Chem. Mater.*, 2017, **29**, 9628-9638; F. G. Cirujano, I. Luz, M. Soukri, C. Van Goethem, I. F. J. Vankelecom, M. Lail and D. E. De Vos, *Angew. Chem., Int. Ed.*, 2017, **56**, 13302-13306.
26. M. Kitano, Y. Inoue, M. Sasase, K. Kishida, Y. Kobayashi, K. Nishiyama, T. Tada, S. Kawamura, T. Yokoyama, M. Hara and H. Hosono, *Angew. Chem., Int. Ed.*, 2018, **57**, 2648-2652; P. Peng, Y. L. Cheng, R. Hatzenbeller, M. Addy, N. Zhou, C. Schiappacasse, D. J. Chen, Y. N. Zhang, E. Anderson, Y. H. Liu, P. Chen and R. Ruan, *Int. J. Hydrog. Energy*, 2017, **42**, 19056-19066; M. Hara, M. Kitano and H. Hosono, *ACS Catal.*, 2017, **7**, 2313-2324.

